Check for updates

Micelle carriers based on dendritic macromolecules containing bis-MPA and glycine for antimalarial drug delivery†

Elisabet Martí Coma-Cros,‡[a,b,c] Alexandre Lancelot, [ID] ‡[d] María San Anselmo,[d] Livia Neves Borgheti-Cardoso, [ID] [a,b,c] Juan José Valle-Delgado,[e] José Luis Serrano, [ID] *[d,f] Xavier Fernàndez-Busquets [ID] *[a,b,c] and Teresa Sierra [ID] *[f]

Biomaterials for antimalarial drug transport still need to be investigated in order to attain nanocarriers that can tackle essential issues related to malaria treatment, *e.g.* complying with size requirements and targeting specificity for their entry into *Plasmodium*-infected red blood cells (pRBCs), and limiting premature drug elimination or drug resistance evolution. Two types of dendritic macromolecule that can form vehicles suitable for antimalarial drug transport are herein explored. A new hybrid dendritic-linear-dendritic block copolymer based on Pluronic® F127 and amino terminated 2,2′-bis(glycyloxymethyl)propionic acid dendrons with a poly(ester amide) skeleton (HDLDBC-bGMPA) and an amino terminated dendronized hyperbranched polymer with a polyester skeleton derived from 2,2′-bis(hydroxymethyl)propionic acid (DHP-bMPA) have provided self-assembled and unimolecular micelles. Both types of micelle carrier are biocompatible and exhibit appropriate sizes to enter into pRBCs. Targeting studies have revealed different behaviors for each nanocarrier that may open new perspectives for antimalarial therapeutic approaches. Whereas DHP-bMPA exhibits a clear targeting specificity for pRBCs, HDLDBC-bGMPA is incorporated by all erythrocytes. It has also been observed that DHP-bMPA and HDLDBC-bGMPA incorporate into human umbilical vein endothelial cells with different subcellular localization, *i.e.* cytosolic and nuclear, respectively. Drug loading capacity and encapsulation efficiencies for the antimalarial compounds chloroquine, primaquine and quinacrine ranging from 30% to 60% have been determined for both carriers. The resulting drug-loaded nanocarriers have been tested for their capacity to inhibit *Plasmodium* growth in *in vitro* and *in vivo* assays.

Introduction

According to the latest estimates, around 219 million cases of malaria occurred globally in 2017 and the disease led to 435 000 deaths.[1] People living in the poorest countries are the most vulnerable, with approximately 90% of deaths in Africa, of which 70% are children under 5 years of age. Although increased prevention and control measures have led to a reduction in malaria mortality rates by more than 42% globally since 2000, an estimated 3.4 billion people are still at risk of being infected and developing disease. Despite the undeniable importance of malaria elimination on the global research agenda, current vaccines in development do not offer prospects of complete protection[2] and the available front-line drugs are rapidly losing efficacy, with resistance already evolved to the first-line drug artemisinin.[3] As a result, since 2014 the malaria incidence and mortality decline have stalled. Thus, alternative strategies[4] working through radically new mechanisms are urgently needed. Antimalarial drugs can potentially target a suite of pathogen life stages inside two different hosts: humans and the insect vector. Infection starts when a parasitized female *Anopheles* mosquito, while taking a blood meal, inoculates sporozoites of the malaria parasite, the

[a]*Nanomalaria Group, Institute for Bioengineering of Catalonia (IBEC), The Barcelona Institute of Science and Technology, Baldiri Reixac 10-12, ES-08028 Barcelona, Spain. E-mail: xfernandez_busquets@ub.edu*
[b]*Barcelona Institute for Global Health (ISGlobal, Hospital Clínic-Universitat de Barcelona), Rosselló 149-153, ES-08036 Barcelona, Spain*
[c]*Nanoscience and Nanotechnology Institute (IN2UB), University of Barcelona, Martí i Franquès 1, ES-08028 Barcelona, Spain*
[d]*Instituto de Nanociencia de Aragón (INA), Química Orgánica, Facultad de Ciencias, Universidad de Zaragoza, Spain. E-mail: joseluis@unizar.es*
[e]*Department of Bioproducts and Biosystems, School of Chemical Engineering, Aalto University, PO Box 16300, FI-00076 Aalto, Finland*
[f]*Instituto de Ciencia de Materiales de Aragón (ICMA), Facultad de Ciencias, Universidad de Zaragoza-CSIC, Spain. E-mail: tsierra@unizar.es*
†Electronic supplementary information (ESI) available. See DOI: 10.1039/c8bm01600c
‡These authors contributed equally.

protist *Plasmodium* spp. In the liver, sporozoites develop into merozoites,[5] which enter the circulation, invade red blood cells (RBCs)[6] and replicate asexually through ring, trophozoite and schizont stages to produce daughter cells that invade new RBCs to perpetuate the blood-stage cycle. Some parasites eventually differentiate into sexual stages, female or male gametocytes that are ingested by a mosquito from peripheral blood. Following fertilization in the insect's midgut, the zygote differentiates into an ookinete that moves through the midgut epithelium and forms an oocyst, which releases sporozoites. The malaria transmission cycle is restarted when sporozoites migrate to the salivary glands and are injected into a human with the mosquito's next bite.

Most chemotherapeutic approaches against malaria are targeted at the asexual, blood-stage parasites that are responsible for all symptoms and pathologies of the disease.[7] Currently administered antimalarial drugs are in free form in the blood circulation and have poor specificity for *Plasmodium*-infected RBCs (pRBCs). This incurs the risk of having to deliver large overall doses over an extended period of time to compensate for drug removal through spleen and liver clearance and kidney filtration. However, patient non-compliance and low concentration thresholds to ward off potential side effects often end up in sublethal local drug amounts reaching infected cells, which in turn stimulate resistance evolution. Because malaria pathophysiology is so complex and the disease is so widespread, it is generally accepted that to achieve eradication a combination of weapons will be needed.[8] These include the improvement of existing approaches and the development of new ones,[9] with drug therapy remaining the mainstay of treatment and prevention,[10] and nanotechnology being able to provide innovative useful tools.[11] The objective of delivering drugs exclusively to a selected site with minimal exposure for sensitive adjacent healthy cells or tissues is the holy grail of the fast-developing nanomedicine field.[12] Encapsulation of drugs in targeted nanovectors is a rapidly growing area with a clear applicability to infectious disease treatment,[13] and pharmaceutical nanotechnology has been identified as a potentially essential asset to the future fight against malaria.[14,15]

In the search for suitable nanocarriers for the treatment of infectious diseases, dendrimers stand out as valuable candidates due to their inherent features for building nanostructures with controlled size, morphology and surface functionalization.[16] In a previous work we had explored different amphiphilic cationic dendritic derivatives based on 2,2′-bis(hydroxymethyl)propionic acid (bis-MPA)[17] as nanocarriers for the targeted delivery of antimalarial drugs.[18] These dendritic derivatives consisted of Janus dendrimers[19] or hybrid dendritic-linear-dendritic block copolymers (HDLDBC),[20] and both self-assembled into micelles with glycine groups at the surface. Although some of these structures exhibited specific pRBC targeting and *in vitro* antimalarial activity, they had an excessive unspecific toxicity, a very large size after antimalarial drug loading (>150 nm), and their *in vivo* tests had been preliminary.

Here we build on our previous work to explore new specifically targeted delivery systems for antimalarial drugs of a size after drug encapsulation (<30 nm) sufficiently small to facilitate their entry into pRBCs.[21] Accordingly, two types of cationic dendritic derivative are proposed, which mainly differ in the way they form the nanocarrier, either self-assembled micelles or unimolecular micelles. As for the former, and on the basis of the promising results shown by the previously reported Pluronic® F127 HDLDBC derivative that contained polyester dendrons,[18] we have herein conjugated Pluronic® F127 with poly(ester amide) dendrons to generate a new micelle-forming self-assembling amphiphilic cationic HDLDBC (Fig. 1A). The combination of the hydrolytic degradability of ester linkages and the stability and H-bond-forming ability of amide groups has proven very interesting for the design of synthetic polymers for biomedical applications.[22,23] Accordingly, a poly(ester amide) dendron conjugated at both ends of Pluronic® F127 has been herein envisaged as a possibility to modulate the size and stability of self-assembled micelles given the additional H-bonding interactions due to amide groups. The dendron employed derives from the monomer 2,2′-bis(glycyloxymethyl)propionic acid (bis-GMPA), which was recently described by us as one of the few examples of poly(ester amide) dendritic structures reported in the literature, which showed high potential for biomedical applications due to the biocompatibility, degradability and positive results in drug and gene delivery of its dendritic derivatives.[24] As for the achievement of a unimolecular micelle carrier, we have
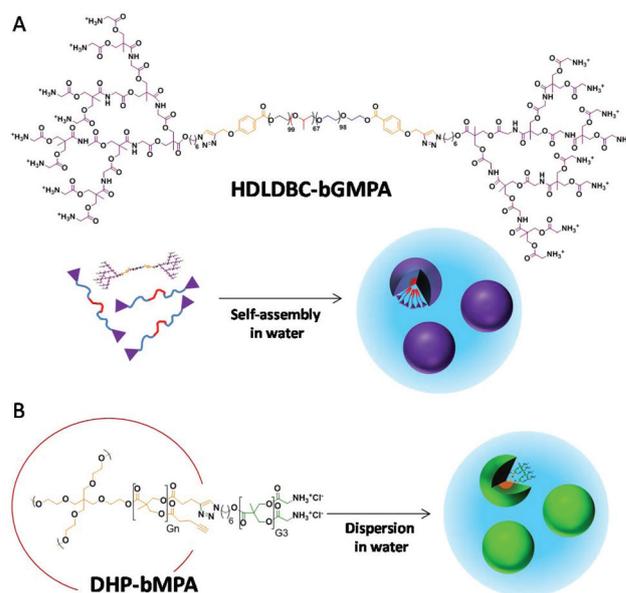

Fig. 1 Chemical structure and cartoon representation of (A) micelle formation by HDLDBC-bGMPA, a hybrid dendritic-linear-dendritic block copolymer composed by Pluronic F127 and dendrons derived from 2,2′-bis(glycyloxymethyl)propionic acid (bis-GMPA), and (B) DHP-bMPA, dendronized hyperbranched polymers derived from 2,2′-bis(hydroxymethyl) propionic acid (bis-MPA) hyperbranched polymers and bis-MPA dendrons functionalized with glycine groups.

selected dendronized hyperbranched polymers (DHPs), also called pseudo-dendrimers, based on a hyperbranched polymer of bis-MPA, conjugated at its periphery with bis-MPA dendrons with exposed glycine moieties (Fig. 1B). We demonstrated that these DHP-bMPA derivatives could deliver DNA into mesenchymal cells.[25] However, their potential as drug carriers remains to be explored. In this respect, these polymers showed appropriate biocompatibility and degradability that make them interesting to be investigated as carriers for antimalarial drug delivery.

Both types of structure have been investigated for their targeting towards pRBCs, and the drug loading capacity and encapsulation efficiencies of the carriers have been tested with the antimalarial compounds chloroquine (CQ), primaquine (PQ) and quinacrine (QN). The resulting nanocarriers have been assayed for their capacity to inhibit *Plasmodium* growth in *in vitro* and *in vivo* assays.

Materials and methods

Reagents

Unless otherwise indicated, all reagents were purchased from Sigma-Aldrich® or Acros™, and used always without further purification. Dichloromethane (DCM) and tetrahydrofuran (THF) were dried using solvent purification systems.

Synthesis and characterization of the dendritic derivatives

Globular DHP-bMPA dendronized hyperbranched polymers as well as DHP-bMPA-Rho, a DHP containing covalently linked rhodamine B fluorophore, were synthesized as previously reported by us.[25] HDLDBC-bGMPA was prepared by copper azide–alkyne cycloaddition (CuAAC) coupling of the *t*-Boc protected bis-GMPA dendron and the Pluronic® F127 bis(alkyne) derivative as depicted in Fig. 2A.
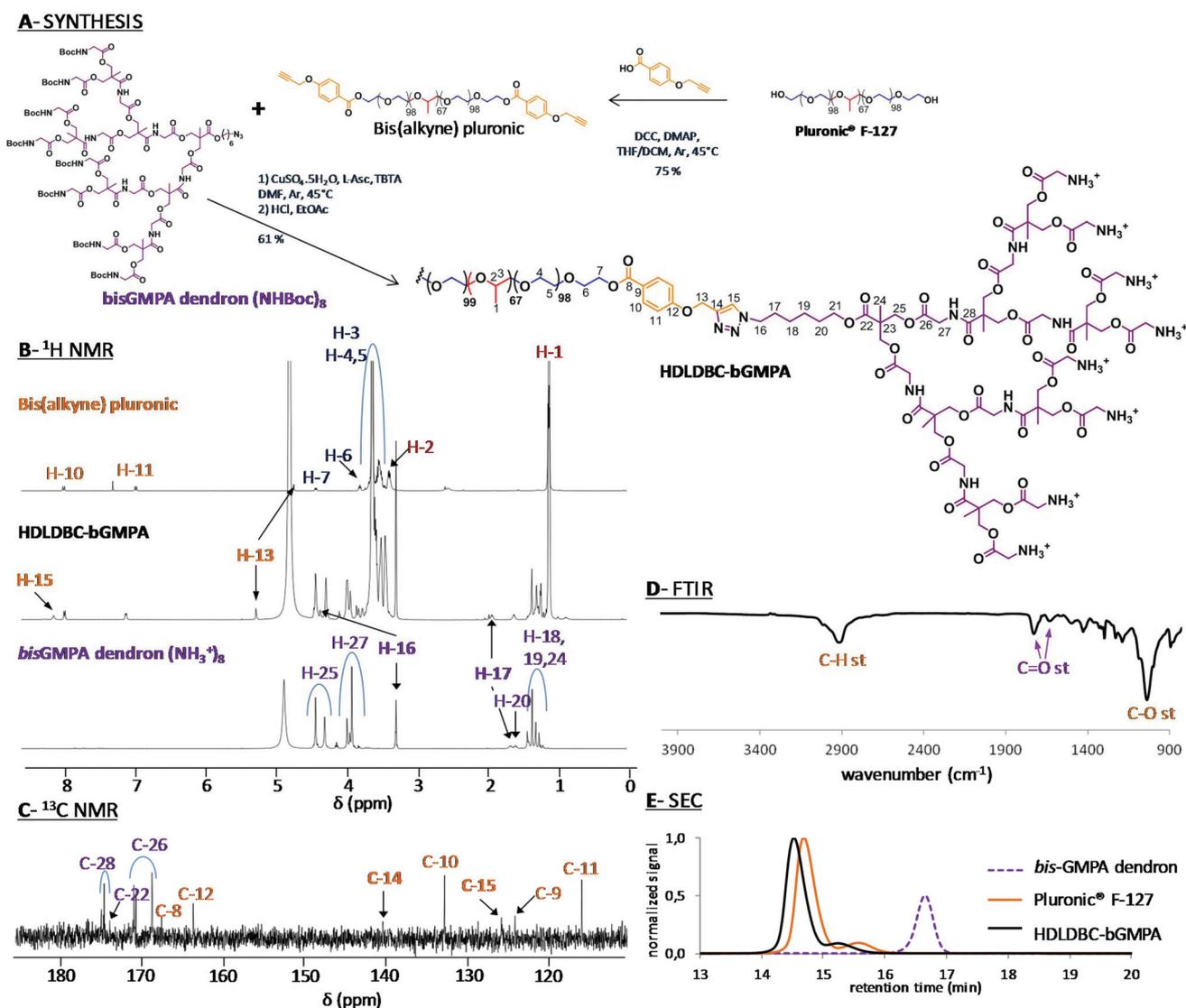

Fig. 2 Synthesis of HDLDBC–bGMPA (A) and chemical characterization by ^{1}H NMR (B), ^{13}C NMR (C), FTIR (D) and SEC (E). ^{1}H NMR spectra with signal relative integration, the ^{1}H–^{1}H COSY NMR spectra and full ^{13}C NMR spectra of HDLDBC–bGMPA are gathered in the ESI.†

Synthetic procedure and analytical data of *t*-Boc protected HDLDBC-bGMPA. Alkyne functionalized Pluronic® F127 (1.00 g, 7.74×10^{-2} mmol, 1.00 eq.) and bis-GMPA dendron (NHBoc)$_8$ (514 mg, 2.01×10^{-1} mmol, 2.60 eq.) were dissolved into 8 mL of dimethylformamide (DMF) in a Schlenk flask and 3 vacuum–argon cycles were made to remove the air. The reaction mixture was stirred under argon atmosphere at 45 °C. CuSO$_4$·5H$_2$O (18.2 mg, 6.19×10^{-2} mmol, 0.80 eq.), (L)-ascorbate (24.1 mg, 1.24×10^{-1} mmol, 1.60 eq.) and tris[(1-benzyl-1*H*-1,2,3-triazol-4-yl)methyl]amine (TBTA, 32.8 mg, 6.19×10^{-2} mmol, 0.80 eq.) were dissolved into DMF (4 mL) in a second Schlenk flask and exposed to 3 vacuum–argon cycles. The copper solution was stirred under argon atmosphere at 45 °C for 15 min and was added through a cannula to the previous azide–alkyne reaction. The resulting mixture was stirred under argon atmosphere at 45 °C for 2 days. Then, hot brine (100 mL) was added to the reaction mixture and the product was extracted with dichloromethane (3 × 100 mL). The organic phases were collected, washed with hot brine (2 × 100 mL), dried over anhydrous MgSO$_4$ and the solvent was evaporated under reduced pressure to obtain a yellow solid. The crude product was precipitated into cold diethyl ether, recovered by filtration and washed with cold diethyl ether to yield a white powder. Finally, the product was dialyzed (cellulose membrane, 1000 Da cut-off, Spectra/Por®) against methanol for 24 h to obtain a light yellow solid (855 mg, 61%). ^{1}H NMR (400 MHz, CDCl$_3$) δ (ppm): 1.11 (m, 201H), 1.26 (m, 42H), 1.41 (m, 152H), 1.62 (m, 4H), 1.94 (m, 4H), 3.38 (m, 67H), 3.44–3.74 (m, ~1000H), 3.81 (t, J = 4.8 Hz, 4H), 3.88 (m, 32H), 3.94 (m, 8H), 3.88 (m, 16H), 4.11 (t, J = 6.4 Hz, 4H), 4.18–4.35 (m, 60H), 4.43 (t, J = 4.8 Hz, 4H) 5.29 (s, 4H), 5.35 (bs), 7.02 (d, J = 8.8 Hz, 4H), 7.17 (bs), 7.82 (s, 2H), 8.00 (d, J = 8.0 Hz, 4H). FTIR (ν_{max}/cm^{-1}): 3360 (N–H st), 2883 (C–H st), 1755 (C=O st ester), 1718 (C=O st carbamate), 1670 (C=O st amide), 1533 (N–H δ), 1468 (CH$_2$, –CH$_3$ δ), 1101 (C–O–C st). SEC (ref PMMA): 2 populations; M_w 19 745 g mol^{-1}; $Đ$: 1.08.

Cleavage of *t*-Boc protecting groups and analytical data of HDLDBC-bGMPA. *t*-Boc protected HDLDBC-bGMPA (653 mg, 3.62×10^{-2} mmol, 1.00 eq.) was dissolved into ethyl acetate (3 mL), and a saturated solution of HCl$_{(g)}$ (7 mL) in ethyl acetate was carefully added to it. The reaction was stirred at room temperature for 45 min until a white gel appeared. The mixture was diluted with ethyl acetate (40 mL) and was stirred for an additional 30 min. Then, it was stirred under vacuum to remove the hydrochloric acid and the solvent was evaporated under reduced pressure. The gel was washed first with pure ethyl acetate and subsequently with pure methanol. In each case, the solution was stirred for 15 min under vacuum in order to remove the residual hydrochloric acid traces and then, the solvent was evaporated under reduced pressure to obtain a solid (615 mg, quantitative). ^{1}H NMR (500 MHz, CD$_3$OD) δ (ppm): 1.14 (m, 201H), 1.27 (s, 6H), 1.32 (s, 20H), 1.39 (s, 24H), 1.64 (m, 4H), 1.95 (m, 4H), 3.47 (m, 67H), 3.51–3.73 (m, ~1000H), 3.84 (t, J = 4.8 Hz, 4H), 3.96 (s, 8H), 4.00 (s, 16H), 4.03 (s, 32H), 4.12 (t, J = 6.0 Hz, 4H), 4.31 (m, 24H), 4.45 (m, 40H) 5.30 (s, 4H), 7.38 (d, J = 8.8 Hz, 4H), 8.23 (d, J = 8.8 Hz,

4H), 8.19 (s, 2H). ^{13}C NMR (125 MHz, CD$_3$OD) δ (ppm): 17.4–18.3, 26.3, 26.9, 29.3, 31.1, 41.5, 42.2, 47.3, 51.3, 62.6–76.8, 115.9, 124.2, 125.8, 132.8, 140.4, 163.7, 167.6, 168.8, 170.8–171.2, 174.0, 174.7–175.0. FTIR (ν_{max}/cm^{-1}): 3600–3300 (bs N–H$^+$), 2885 (C–H st), 1751 (C=O st ester), 1663 (C=O st amide and N–H$^+$ δ), 1545 (N–H δ), 1468 (CH$_2$–, CH$_3$ δ), 1099 (C–O–C st).

Characterization techniques. ^{1}H and ^{13}C Nuclear Magnetic Resonance (NMR) experiments were performed using a Bruker AV-400 (^{1}H: 400 MHz, ^{13}C: 100 MHz) or a Bruker AV-500 (^{1}H: 500 MHz, ^{13}C: 125 MHz) spectrometer (Bruker Corporation, Billerica, MA, USA), employing as solvents deuterated chloroform (CDCl$_3$), deuterated methanol (CD$_3$OD) or deuterated dimethyl sulfoxide ((CD$_3$)$_2$SO). The chemical shifts are indicated in ppm relative to tetramethylsilane (TMS) and the coupling constant in Hz; the solvent residual peak was used as internal standard for spectrum calibration. Fourier transformed infrared (FTIR) spectroscopy was performed using a Bruker Vertex 70 spectrophotometer in ATR (attenuated total reflectance) mode and recorded between 4000 and 800 cm^{-1}. Size exclusion chromatography (SEC) was performed with a Walter e2695 Alliance employing two in series HR4 and HR1 Styragel columns (500 and 10^4 Å of pore size, respectively) and a Waters 2424 evaporation light scattering detector with a sample concentration of 1 mg mL^{-1} in THF (HPLC grade) with a flow rate of 1 mL min^{-1} at 35 °C; poly(methyl methacrylate), PMMA, was used as standard for calibration.

Self-assembly of HDLDBC-bGMPA

HDLDBC-bGMPA was mixed with the corresponding amount of distilled water and cooled down to 4 °C for 30 min until complete dissolution. Then, the solution was slowly heated to room temperature to trigger the formation of the water soluble nanocarriers. The critical micelle concentration (CMC) was determined using the Nile Red technique.[26] Briefly, 2 mL of distilled water solutions of HDLDBC-bGMPA with concentrations ranging from 0.1 to 5 mg mL^{-1} were prepared at 25 °C. Nile Red was dissolved in ethanol at a concentration of 0.25 mM and 10 μL of this solution was added to each sample. The mixtures were then stirred at room temperature for 1 h in the dark with an orbital shaker. The fluorescence emission spectrum of each solution was recorded with a PerkinElmer LS 55 fluorimeter after excitation at λ_{ex} = 550 nm.

Preparation of carrier-antimalarial drug conjugates and drug release assays

The antimalarial compounds CQ, PQ and QN were encapsulated within the corresponding carrier (DHP-bMPA or HDLDBC-bGMPA) following the oil-in-water procedure previously employed by us for CQ and PQ.[18] Briefly, each dendritic derivative and the corresponding drug were dissolved into a mixture of DCM and distilled water (1 : 1) at feeding ratios of $w_{DHP} : w_{drug}$ = 1 : 0.5 and $w_{HDLDBC} : w_{drug}$ = 1 : 1. The samples were vigorously stirred at room temperature employing an orbital shaker under ventilation until complete evaporation of DCM (around 2 h). Non-encapsulated drug was removed by

dialysis (regenerated cellulose membrane, MW 1000 Da cut off, Spectra/Por®) against distilled water (200 mL) at 4 °C for 16 h. The amount of encapsulated drug was indirectly determined: the quantity of drug present in the dialysis water was measured by UV-VIS spectrometry (Varian Cary50 Probe UV-visible spectrophotometer) at the wavelengths of $\lambda_{A(CQ)}$ = 345 nm for CQ, $\lambda_{A(PQ)}$ = 259 nm for PQ and $\lambda_{A(QN)}$ = 280 nm for QN and was subtracted from the initially incorporated drug. The samples were freeze-dried with a Telstar Cryodos 50 freeze-dryer in order to increase their stability over long storage periods.

The release of CQ encapsulated within HDLDBC-bGMPA and DHP-bMPA was studied by dialysis against phosphate buffered saline (PBS). 2 mL of the dendrimer/drug conjugates were dialyzed against 200 mL of PBS (regenerated cellulose dialysis membrane, MW 1000 Da cut-off, Spectra/Por®) under stirring at 37 °C. For CQ determination, aliquots (2 mL) were withdrawn at different times from the waters of dialysis up to 72 h (specifically at 0, 2, 4, 6, 24, 48, and 72 h). An identical procedure was performed with a control solution of free CQ at the same concentration as in the conjugate preparation.

Fluorescent labeling of HDLDBC-bGMPA

HDLDBC-bGMPA nanocarriers were labeled by encapsulating a low water soluble modified rhodamine B (Rho(C17)$_2$) red fluorophore previously reported by us,[27] and the oil-in-water procedure was employed to encapsulate the fluorophore within the nanocarrier. The selected feeding ratio in this case was (1 : 0.15) (w_{HDLDBC} : w_{Rho}). The release profile of Rho(C17)$_2$ from the dendrimer/Rho(C17)$_2$ conjugates was studied by dialysis similarly as the drug release procedure described above. In this case, 2 mL of the HDLDBC-bGMPA/Rho(C17)$_2$ conjugate containing 0.15 mg mL^{-1} of encapsulated Rho(C17)$_2$ were dialyzed (regenerated cellulose membrane, MW 2000 Da cut off, Spectra/Por®) against distilled water (200 mL) at 37 °C. At different times up to 72 h, 2 mL aliquots were withdrawn from where the quantity of Rho(C17)$_2$ was determined by measuring fluorescence intensity (λ_{ex} = 540 nm, λ_{em} = 580 nm).

Transmission electron microscopy (TEM) and atomic force microscopy (AFM) analysis

TEM images were obtained with a FEI TECNAI T20 electron microscope (FEI Company, Eindhoven, The Netherlands) with 200 kV beam power, using holey carbon film 300 mesh coppered grids (Agar Scientific Ltd). A droplet of an aqueous solution of the sample at a concentration of 1 mg mL^{-1} was deposited on the grid and let to adsorb for 30 s, removing the excess aqueous solution by blotting with filter paper. A droplet of a 3% w/v aqueous solution of phosphotungstic acid used as negative stain was deposited on the grid and left for 10 s before removing the excess staining solution by blotting with filter paper. The grid was dried for at least 24 h under atmospheric pressure at room temperature. The average size of the different nanocarriers was obtained by analysing ≥100 structures in ≥4 TEM images.

For AFM analyses, 10 μL of 1 μg mL^{-1} or 10 ng mL^{-1} dendrimer solution in double deionised water (ddH$_2$O; MilliQ system, Millipore) were deposited on cleaved mica substrates and, after an adsorption time of about 5 min, 40 μL ddH$_2$O were added. High-resolution images were obtained with a MultiMode 8 atomic force microscope equipped with a NanoScope V controller (Bruker Corporation) operating in ScanAsyst mode in liquid, using ScanAsyst-Fluid + probes (Bruker Corporation).

Plasmodium falciparum cell culture and parasite growth inhibition assay

P. falciparum 3D7 was grown *in vitro* in human RBCs of blood group type B prepared as described elsewhere[28] using previously established conditions.[29] Briefly, parasites (thawed from glycerol stocks) were cultured at 37 °C in T25 flasks (SPL Life Sciences) containing RBCs in Roswell Park Memorial Institute (RPMI) complete medium (supplemented with 5 g L^{-1} Albumax II and 2 mM glutamine) under a gas mixture of 92% N$_2$, 5% CO$_2$, and 3% O$_2$. Synchronized ring stage cultures were obtained by 5% sorbitol lysis and synchronized late stage cultures were obtained using 70% Percoll® (GE Healthcare) purification to enrich in late trophozoites and early schizonts;[30] the medium was changed every 2 days maintaining 3% hematocrit. For culture maintenance, parasitemias were kept below 5% late forms by dilution with fresh RBCs. The human blood used in this work was commercially obtained from the *Banc de Sang i Teixits* (http://www.bancsang.net). Blood was not specifically collected for this research; the purchased units had been discarded for transfusion, usually because of an excess of blood relative to anticoagulant solution. Prior to their use, blood units underwent the analytical checks specified in the current legislation. Before being delivered to us, unit data were anonymized and irreversibly dissociated, and any identification tag or label had been removed in order to guarantee the non-identification of the blood donor. No blood data were or will be supplied, in accordance with the current *Ley Orgánica de Protección de Datos* and *Ley de Investigación Biomédica*. The blood samples will not be used for studies other than those made explicit in this research. Experiments were approved by the Ethics Committee of the *Hospital Clínic de Barcelona*.

To isolate *P. falciparum* merozoites, a 3D7 strain culture was tightly synchronized (sorbitol lysis on day 1, 70% Percoll® followed after 2 h by sorbitol on day 4, sorbitol on day 6), and after a further 40 h a final 70% Percoll® treatment was done. Purified late stages were cultured in 10 mL of complete RPMI without adding fresh RBCs, and when the majority of parasites were segmented schizonts, E-64 protease inhibitor was added to a final concentration of 10 μM. Between 6 to 10 h later, the culture was centrifuged at 730g for 8 min and the pelleted cells were taken up in 20 mL of PBS. The suspension was passed sequentially through a 18G needle and a 1.2 μm filter (Sartorius Stedim® Minisart) blocked for 30 min with PBS/1% BSA. Merozoites in PBS were collected in a 50 mL Falcon tube previously blocked for 1 h with PBS/1% BSA, and finally centri-

fuged at 2200g for 10 min. The supernatant was removed leaving about 200 μL of a merozoite suspension in PBS, which was immediately used for targeting analysis.

For growth inhibition assays, *P. falciparum* 3D7 cultures were adjusted to 3% hematocrit and 1.5% parasitemia with more than 90% of parasites at ring stage after sorbitol synchronization. 75 μL of these *Plasmodium* cultures were plated in 96-well plates and incubated for 40 h at 37 °C in the presence of free drugs and dendrimer–drug conjugates (added in a volume of 75 μL). After addition of 0.5 μM Syto-11 (Thermo Fisher Scientific, Inc.), parasitemia was determined by flow cytometry as previously described.[28]

Cytotoxicity and hemolysis assays

Human umbilical vein endothelial cells (HUVEC, ATCC) were cultured in Medium 199 (M199, LabClinics) supplemented with 10% heat-inactivated foetal bovine serum (FBS, PAA Laboratories, Germany), 1% each penicillin/streptomycin (Biological Industries), and 10 mM glutamine (complete M199). 5000 cells per well were plated in 96-well plates (Thermo Fisher Scientific Inc.) and after 24 h at 37 °C in 5% CO_2 atmosphere the medium was substituted by dilutions of the dendrimers in 100 μL of culture medium without FBS, and incubation was resumed for 48 h. 10 μL of 4-[3-(4-iodophenyl)-2-(4-nitrophenyl)-2H-5-tetrazolio]-1,3-benzene disulfonate labeling reagent (WST-1, Roche Diagnostics GmbH) was added to each well, and the plate was incubated in the same conditions for a further 3 h. After thoroughly mixing for 1 min on a shaker, the absorbance of the samples was measured at 440 nm using a Benchmark Plus microplate reader (Bio-Rad Laboratories Inc.). WST-1 in the absence of cells was used as blank and samples were prepared in triplicate for each experiment, including positive (10% bleach) and negative (PBS) controls.

For hemolysis assays, human blood collected in citrate-phosphate-dextrose buffer was washed as described previously.[28] After the last washing step RBCs were diluted in PBS to yield a solution with 6% hematrocrit. 100 μL of RBCs from this suspension and 100 μL of a dendrimer sample were added to a 96-well plate. Each assay was performed in triplicate, including positive (1% Triton X-100) and negative (PBS) controls. After incubating for 3 h at 37 °C in 90% N_2, 5% CO_2, and 5% O_2, samples were collected in eppendorf tubes, spun at 16 000g for 5 min, and the supernatant absorbance was finally measured at 541 nm.

Cell targeting analysis

400 μL of desynchronized living *P. falciparum* 3D7 cultures were stained for 30 min with 4 μg mL^{-1} of the DNA dye Hoechst 33342. HUVEC (1.5 × 10^4 cells per cm^2) were treated equally but for the use of complete M199 as culture medium, and nuclei staining done at day 3 after plating (10 μg Hoechst 33342 per mL). After 3 washes with complete RPMI or M199, respectively, *Plasmodium* cultures and HUVEC were incubated in the presence of 0.15 mg mL^{-1} dendrimer conjugated to rhodamine, for 90 min in the corresponding medium at 37 °C

with gentle stirring. Purified merozoites were incubated for 10 min at room temperature (RT) in the simultaneous presence of Hoechst 33342 and rhodamine-labeled dendrimers. After washing with incomplete medium, nonfixed samples were placed in a 8-well LabTek chamber slide system (Lab-Tek®II, catalog number 155409) and the fluorescence of Hoechst 33342, FITC and rhodamine ($\lambda_{ex/em}$: 350/461, 488/520 and 553/627 nm, respectively) was observed with an IX51 inverted fluorescence microscope (Olympus). Confocal fluorescence microscopy analysis was done with a Leica TCS SP5 laser scanning confocal microscope equipped with a DMI6000 inverted microscope, blue diode (405 nm), Argon (458/476/488/496/514 nm), diode pumped solid state (561 nm) and Helium–Neon (594/633 nm) lasers and PLAN APO 63× oil (NA 1.4) immersion objective lens. For flow cytometry analysis, *Plasmodium* cultures were diluted in PBS to a final concentration of 1–10 × 10^6 cells per mL, and samples were analyzed using a LSRFortessa™ flow cytometer instrument (BD Biosciences) set up with the 5 lasers, 20 parameters standard configuration. The single-cell population was selected on a forward-side scatter scattergram. Rhodamine was excited using a yellow-green laser (561 nm), and its fluorescence collected through a 582/15 nm filter. Hoechst 33342 was excited with a violet laser (405 nm), and its fluorescence collected using a 450/40 nm filter.

Determination of the maximum tolerated dose (MTD) in mice

Seven week-old inbred BALB/cAnR mouse females (18–20 g, Janvier Laboratories) were maintained under standard environmental conditions (20–24 °C and 12 h/12 h light/dark cycle) with *ad libitum* access to food and water. To ensure administration and minimize injection stress, the animals were anesthetized with isoflurane (4% for induction and 2.5% for maintenance) in an oxygen stream, while a 250 μL bolus was administered intravenously. To reduce the number of animals used, an adaptation of OECD 425 Test Guideline was followed, which consisted of a single ordered dose progression. The first mouse received the dose initially planned for antimalarial activity assays (see below), and the dose for the next animal was either increased or decreased by a factor of 3.2 depending on whether the first animal survived or died, respectively. Each mouse was injected and evaluated for at least 48 h before the next animal was treated. All animals were observed for toxic signs during 14 days after dose injection. Following this protocol, three different concentrations of the dendrimers (11.7, 37.5 and 120 mg kg^{-1}) were evaluated, prepared in PBS from a 50 mg mL^{-1} stock solution of dendrimers in sterile ddH$_2$O. In the presence of toxic effects including, among others, >20% reduction in animal weight, aggressive and unexpected animal behavior or the presence of blood in faeces, animals were immediately anesthetized using a 100 mg kg^{-1} Ketolar plus 5 mg kg^{-1} Midazolan mixture and sacrificed by cervical dislocation. Dendrimer MTD was therefore defined upon completion of the assay as the highest dosage exhibiting an absence of the aforesaid toxicity signs. The animal care and use protocols followed adhered to the specific national and

international guidelines specified in the Spanish Royal Decree 53/2013, which is based on the European regulation 2010/63/UE. The studies reported here were performed under protocols reviewed and approved by the Ethical Committee on Clinical Research from the Hospital Clínic de Barcelona (Reg. HCB/2014/0910).

Antimalarial activity assay *in vivo* and dot-blot assays

The *in vivo* antimalarial activity of free CQ and of dendrimer-CQ conjugates was analyzed in a 4-day blood suppressive test as previously described.[31] Briefly, BALB/c mice were inoculated intraperitoneally with 2×10^6 RBCs from *Plasmodium yoelii yoelii* 17XL (PyL) MRA-267-infected mice. Treatment started 4 h later (day 0) with a single dose of 1.9 mg CQ per kg per day administered intravenously as diphosphate–drug or dendrimer–drug, followed by identical dose administration for the next 3 days. Tested compounds were prepared in PBS and the control groups received PBS. Parasitemia was monitored daily by microscopic examination of Giemsa-stained thin blood smears using the Plasmoscore 1.3 software (Burnet Institute, Melbourne, Australia). When all surviving animals had completely cleared *Plasmodium* infection they were re-infected (on day 69) with *P. yoelii yoelii* 17XL (PyL) MRA-267 as above and left untreated. Survival was monitored until day 90, when blood samples (400 μL) were collected on 10 μL of 10% EDTA, centrifuged for 5 min (470g), and the obtained plasma supernatants were stored at −20 °C. 3 μL of *P. yoelii yoelii* 17XL (PyL) MRA-267 extracts[32] containing 1.5 μg protein were applied and allowed to dry on a nitrocellulose membrane (0.45 μm, Bio-Rad, catalog number 1620145). Non-specific sites were blocked with 5% BSA in TBS-T (0.05% Tween 20, 150 mM NaCl, 20 mM Tris-HCl, pH 7.5) for 1 h at RT. Then the membrane was first incubated (30 min, RT) with the plasma supernatants dissolved in TBS-T (1 : 5000 dilution), washed (TBS-T, 3 × 5 min), and then treated with a secondary goat anti-mouse antibody conjugated to horseradish peroxidase (Millipore) in TBS-T (1 : 10 000 dilution; 30 min, RT), followed by 3 × 5 min washes with TBS-T and one wash with TBS (TBS-T without Tween). Finally the membrane was incubated with ECL Prime Western Blotting Detection Reagent (Luminol, Amersham) for 30–60 s and scanned (ImageQuant LAS4000, GE Healthcare).

Statistical analysis

Data are presented as the mean ± standard error of at least three independent experiments, and the corresponding standard errors in histograms and graphs are represented by error bars. Percentages of viability were obtained using non-treated cells as control of survival and IC_{50} values were calculated by nonlinear regression with an inhibitory dose–response model using GraphPad Prism5 software. Concentrations were transformed using natural log for linear regression. Regression models were adjusted for replicates and assay data.

Results and discussion

Preparation and characterization of the nanocarriers

Synthesis and characterization of HDLDBC-bGMPA. HDLDBC-bGMPA was synthesized for the first time for this study by CuAAC of the bis(alkyne) derivative of Pluronic® F127 and two *t*-Boc protected amino-terminated bis-GMPA dendrons (Fig. 2A and ESI†). The *t*-Boc-protected bis-GMPA dendron of 3rd generation with an azide group at the focal point and eight terminal amino groups was synthesized as previously described by us.[24] The synthesis of the alkyne functionalized Pluronic® was carried out by esterification of Pluronic® F127 with 4-(prop-2-ynyloxy)benzoic acid as we reported previously.[18] The CuAAC reaction was performed in DMF at 45 °C under argon atmosphere during 2 days. The Cu(ɪ) catalytic species was formed "*in situ*" by reduction of Cu(ɪɪ) salt with (ʟ)-ascorbate while TBTA was added to increase its stability. An excess of dendron (1.3 mole of dendron per 1.0 mole of alkyne group) was used to obtain a complete functionalization of the linear polymer. The *t*-Boc protecting groups were removed from the dendrons in acidic conditions with HCl in ethyl acetate and the final product was obtained with a moderate yield of 61%.

The correct grafting of the two bis-GMPA dendrons at the extremities of Pluronic® F-127 was first controlled by ^{1}H (Fig. 2B) and ^{13}C (Fig. 2C) NMR experiments (see Fig. S1.1, S1.2 and S1.3† for ^{1}H–^{1}H COSY and full ^{1}H and ^{13}C NMR spectra). The appearance of a peak at 8.19 ppm (H-15) in the ^{1}H NMR spectrum and two peaks at 125.8 (C-15) and 140.4 ppm (C-14) in the ^{13}C NMR spectrum confirmed the formation of the triazole rings. Additionally, three other signals were shifted downfield in the ^{1}H NMR spectra of the final HDLDBC when compared with the spectra of its two precursors. Thus, the signal corresponding to the methylene protons in the α-position of the triazole rings belonging to the linear polymeric part (H-13) was shifted from 4.72 to 5.30 ppm. The signals corresponding to the methylene protons in the α- and β-positions of the triazole rings belonging to the dendritic part (H-16 and H-17) were shifted from 3.20 and 1.65 to 4.45 and 1.95 ppm, respectively. Moreover, the relative integrations of the signals corresponding to the dendrons and linear polymer corroborated the grafting of two dendrons at the terminal position of the Pluronic® F-127 (Table S1.1†).

The characteristic bands of the bis-GMPA dendrons and Pluronic® F-127 could be observed in the FTIR spectrum, (Fig. 2D). First, the presence of the poly(ether) Pluronic® F-127 was asserted by the intense band at 1101 cm^{-1} (C–O bond vibration stretching) and the two intense bands at 2881 and 1344 cm^{-1} (C–H bond vibrations). Second, the presence of the poly(ester amide) bis-GMPA dendrons was confirmed by the two bands at 1755 and 1664 cm^{-1} corresponding to C=O bond vibration stretching of ester and amide groups, respectively.

SEC was performed with the *t*-Boc-protected precursor of HDLDBC-bGMPA due to its low solubility in the elution solvent employed for chromatography, *i.e.* THF (Fig. 2E). Two

peaks were observed in the chromatograms of both, the commercial Pluronic® F-127 and the HDLDBC, showing the polydispersity of these compounds. The correct functionalization of Pluronic® was nevertheless asserted as both peaks corresponding to it showed lower retention time than the two peaks corresponding to the starting Pluronic® F-127. Additionally, no peak corresponding to residual free bis-GMPA dendron could be observed. In summary, all experimental data obtained during the characterization of HDLDBC-bGMPA confirmed the correct insertion of two bis-GMPA dendrons at each extremity of the linear polymer and the absence of unreacted free linear polymer or dendron.

Structural studies. The ability of HDLDBC-bGMPA to self-assemble in water forming micellar nanocarriers was confirmed by CMC determination using the Nile Red method (Fig. 3A). The fluorescence intensity of this solvatochromic fluorophore increases drastically when it migrates into and is retained within the lipophilic part of aggregates formed by the self-assembly of amphiphilic molecules.[26] Thus, a CMC of 1.0 mg mL^{-1} for HDLDBC-bGMPA was determined, which was consistent with the formation of micelles in which the lipophilic core of the central linear Pluronic® block copolymer is sur-

rounded by hydrophilic ammonium terminated dendrons. Rounded structures were observed in AFM and negatively stained TEM images of HDLDBC-bGMPA. The average diameter calculated from TEM micrographs was 13 ± 3 nm, consistent with the height of the structures determined in water by AFM (Fig. 3B and C), and with the average in number value measured by DLS, 26 ± 6 nm (Fig. S2.1.A†).

The morphology of two globular dendronized hyperbranched polymers, DHP-bMPA, was also analyzed by TEM and AFM (Fig. 3D–F). The two generations tested ($n = 3$ and $n = 4$ in Fig. 1B) appeared as rounded objects, with average diameters calculated from TEM images of 9.8 ± 2.7 nm and 13.5 ± 3.5 nm, respectively. These dimensions are consistent with the expected formation by these dendronized hyperbranched polymers of unimolecular micelles well dispersed in aqueous solution.[33,34] DLS measurements of DHP-bMPA ($n = 4$) gave a diameter of 11 ± 2 nm (Fig. S S2.1.B†). As for HDLDBC-bGMPA carriers, the size of DHP-bMPA unimolecular micelles results *a priori* appropriate to enter into pRBCs.[21]

Unspecific toxicity and hemolysis assays. None of the dendritic derivatives was cytotoxic or hemolytic up to a concentration of 0.15 mg mL^{-1} (Fig. 3G and H), which is 10 times higher than the highest amount to be used later for *in vitro* growth inhibition assays, and 8 times higher than the daily dose to be used later for *in vivo* assays.

In vitro targeting analysis

Rhodamine labeling of the nanocarriers. In order to explore the targeting behavior of the nanocarriers towards pRBCs, DHP-bMPA-Rho (Fig. 4A), a DHP-bMPA covalently labeled with an average of seven rhodamine B moieties per macromolecule, was prepared as previously described.[25] HDLDBC-bGMPA nanocarriers were labeled by encapsulating a lipophilic modified rhodamine B (Rho(C17)$_2$) red fluorophore, using the oil-in-water procedure as previously reported by us.[27] In order to check the stability of this labeling, Rho(C17)$_2$ release from the HDLDBC-bGMPA/Rho(C17)$_2$ conjugates was studied by dialysis. Unmodified water-soluble rhodamine B fluorophore was encapsulated within HDLDBC-bGMPA micelles following the same protocol, to be used as a control. The resulting release profiles showed that whereas 50% of the encapsulated rhodamine B is released during the first 2 h, Rho(C17)$_2$ is kept encapsulated throughout the 72 h of the experiment (Fig. 4B).

Erythrocyte targeting analysis. Fluorescence microscopy analysis of non-fixed samples (Fig. 5A) showed that whereas HDLDBC-bGMPA was incorporated by all RBCs, DHP-bMPA exhibited at the same concentration a clear targeting specificity for pRBCs. Higher-resolution confocal fluorescence microscopy images of DHP-bMPA-containing samples revealed that the polymer fluorescence was associated to the pRBC plasma membrane and to intraerythrocytic parasites (Fig. 5B). In the latter case fluorescence was not detected in the RBC cytosol and was circumscribed by the plasma membrane of *Plasmodium*. These observations suggested a specific binding of DHP-bMPA to *Plasmodium falciparum* antigens.
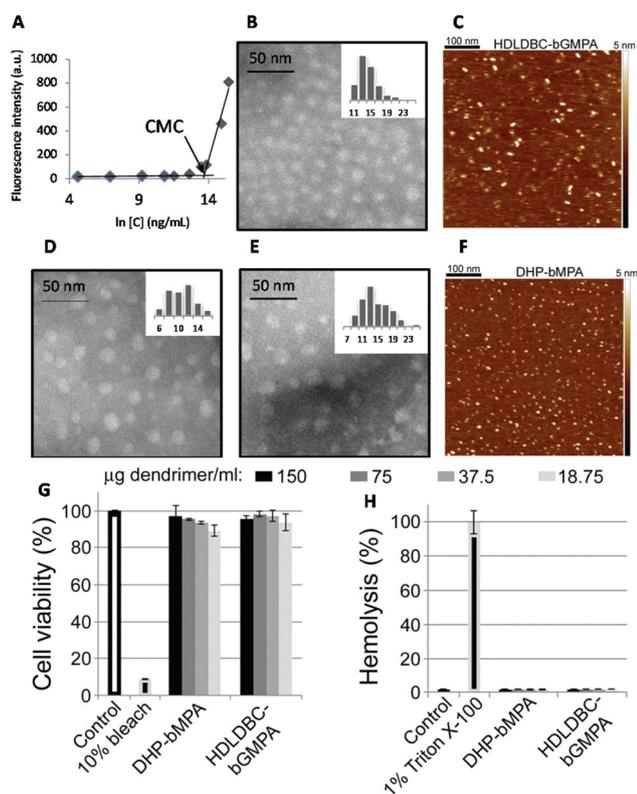

Fig. 3 Characterization of nanocarriers. Nile Red fluorescence intensity as a function of HDLDBC–bGMPA concentration (A), TEM image (B) and AFM image in water on mica surface (C) of HDLDBC–bGMPA, TEM images of DHP-bMPA ($n = 3$ and $n = 4$ in Fig. 1B; D and E, respectively), and AFM image of DHP-bMPA ($n = 4$ in Fig. 1B) in water on mica surface (F). Cytotoxicity (G) and hemolysis assay (H) of the largest DHP-bMPA ($n = 4$ in Fig. 1B) and HDLDBC-bGMPA.
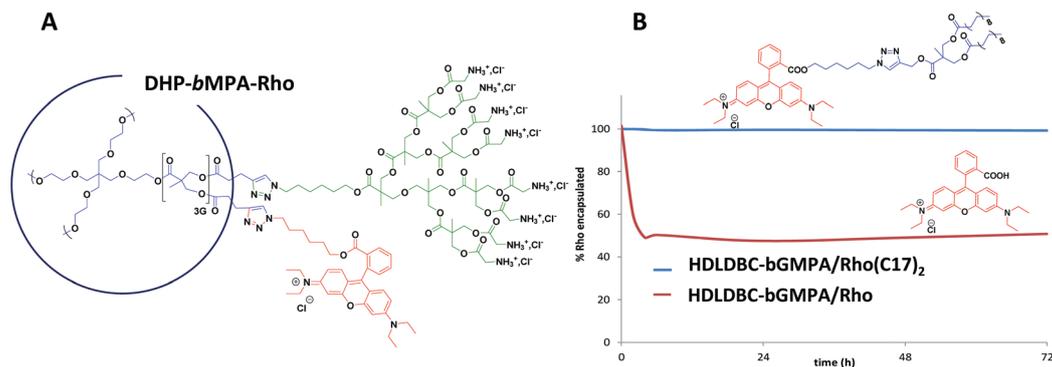
Fig. 4 Rhodamine labeling of the nanocarriers. Chemical structure of the covalently labeled DHP-bMPA-Rho derivative (A), and release profile of the fluorescent rhodamine labels, Rho(C17)$_2$ and Rho, from the nanocarrier HDLDBC-bGMPA (B).
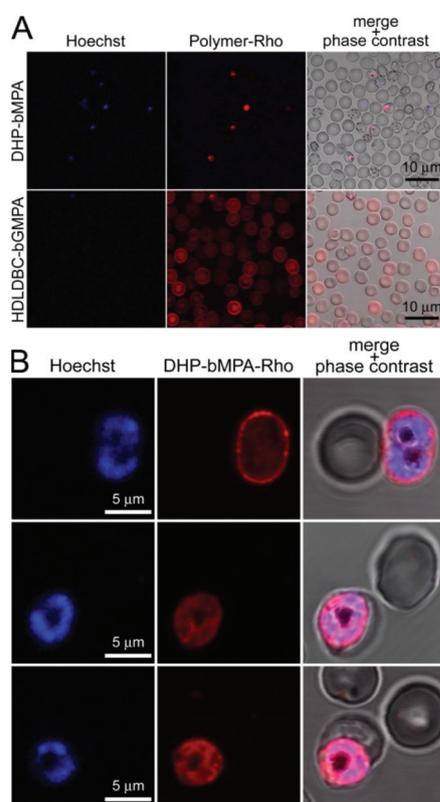

Fig. 5 Fluorescence microscopy cell targeting analysis of rhodamine-labeled DHP-bMPA and HDLDBC-bGMPA to non-fixed RBCs and pRBCs. (A) Conventional fluorescence microscopy cell targeting of both polymers. (B) Confocal fluorescence microscopy cellular and subcellular targeting of DHP-bMPA-Rho.

Fig. 6 Flow cytometry analysis of the targeting of rhodamine-labeled DHP-bMPA and HDLDBC-bGMPA to RBCs, pRBCs and merozoites (the latter two represented in blue, upper left areas; their DNA is stained by Hoechst 33342). pRBCs and merozoites positive for rhodamine are shown in purple (upper right areas) whereas orange (lower right areas) indicates cells or cell debris (the latter only in merozoite samples) lacking DNA that are associated to the polymers. Percentages indicate the fraction of rhodamine-positive counts relative to the total number of recorded cells or particles in each sample. Arrowheads indicate ring stages.

The differential RBC targeting of DHP-bMPA and HDLDBC-bGMPA was confirmed by flow cytometry assays (Fig. 6); whereas HDLDBC-bGMPA associated with *P. falciparum* merozoites and with both parasitized and non-parasitized erythrocytes, DHP-bMPA interacted only with merozoites and with pRBCs. HDLDBC-bGMPA interaction with both RBCs and pRBCs does not invalidate it as a potential carrier of antimalarial drugs in targeted delivery strategies. As we have shown

before, delivering antimalarial compounds to non-infected erythrocytes might represent an interesting therapeutic approach whereby *Plasmodium* would encounter a hostile environment since the very first moment after RBC inva-

sion.[35,36] This scenario resulted in a significantly improved efficacy of drugs encapsulated inside liposomes targeted to both pRBCs and to non-parasitized red blood cells.[35,37]

The modest binding of DHP-bMPA to early ring forms, where the parasite has not significantly modified the erythrocyte membrane, suggests that this polymer might interact predominantly with exported *Plasmodium* antigens, which are scarce in rings and completely absent from non-parasitized RBCs.

Endothelial cell targeting analysis. Other cell types besides RBCs will be exposed to targeted polymers used as drug carriers in the blood stream, mainly leukocytes and blood vessel endothelium. Of these, leukocytes are in numbers several orders of magnitude below those of RBCs, but endothelial cells are sufficiently abundant to compete with pRBCs for nanocarrier intake. We have shown above that, at the polymer concentrations used in this work, endothelial cells do not experience significant cytotoxic effects. However, they might contribute to the clearance from the blood of a significant amount of polymers, thus reducing the efficacy of nanovector preparations. When endothelial cell uptake of the polymers was analyzed by fluorescence microscopy, it was observed that both DHP-bMPA and HDLDBC-bGMPA were incorporated by HUVEC cells. However, whereas HDLDBC-bGMPA had a cytosolic localization, the subcellular targeting of DHP-bMPA was found to be exclusively nuclear (Fig. 7). This result offers interesting perspectives for the use of this type of polymers in the targeting to cell types other than erythrocytes and to different subcellular locations. Nevertheless, the observed interaction of both polymers with the endothelial lining has to be taken into account in future pharmacokinetic studies regarding potential applications as drug carriers against the blood stages of malaria.

In vitro antimalarial activity of drug-loaded nanocarriers

Drug encapsulation. CQ, PQ and QN were encapsulated within DHP-bMPA and HDLDBC-bGMPA nanocarriers. Except where otherwise indicated, the DHP-bMPA structure used here-
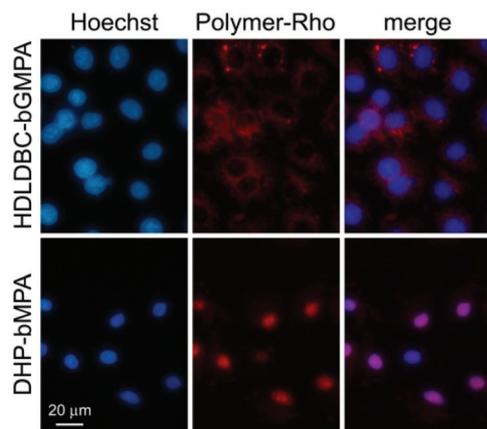

Fig. 7 Fluorescence microscopy cell targeting analysis of rhodamine-labeled DHP-bMPA and HDLDBC-bGMPA to HUVEC cells.

Table 1 Encapsulation of CQ, PQ and QN in HDLDBC-bGMPA and DHP-bMPA nanocarriers and average diameters of the carrier/drug systems determined by TEM

	Drug	mg drug/mg carrier	EE[a] (%)	Average diameter (nm)
HDLDBC-b*G*MPA	Empty			13 ± 3
	CQ	0.307	31	17 ± 3
	PQ	0.408	41	11 ± 2
	QN	0.475	48	14 ± 6
DHP-bMPA	Empty			13.5 ± 3.5
	CQ	0.246	60	20 ± 7
	PQ	0.214	60	19 ± 8
	QN	0.229	37	12 ± 3

[a] Encapsulation efficiency (EE, %) represents the fraction of encapsulated drug relative to the quantity used to perform the encapsulation.

after in this work will be $n = 4$. The encapsulation was performed following the oil-in-water method at feeding ratios of $1:0.5$ (w_{DHP}/w_{drug}) and $1:1$ (w_{HDLDBC}/w_{drug}), respectively. This procedure allowed to encapsulate all three antimalarial drugs in DHP-bMPA nanocarriers with drug loading contents around 20% in weight and good encapsulation efficiencies, ranging from 37% to 60% (Table 1). A smaller DHP-bMPA ($n = 3$ in Fig. 1B) was also used to encapsulate all three antimalarials, obtaining similar drug contents and loading efficiencies (Table S2.1†). As for the HDLDBC-bGMPA carrier, higher loading capacities, between 30% and 48% in weight, and rather good encapsulation efficiencies, ranging from 31% to 48%, were attained.

All the aqueous solutions obtained after the encapsulation procedure were freeze-dried in order to enhance stability during storage of the carrier/drug systems. The effective encapsulation of drugs was asserted by comparing the absorption spectra of the drugs in water with those of the re-dissolved carrier/drug freeze-dried conjugates (Fig. S2.3 and S2.4†). In all cases, the differences observed reflect interactions between nanocarriers and drugs.

TEM images of drug-containing nanocarriers showed in all cases homogeneous dispersions of rounded objects (Fig. 8), the diameters of which were similar to those of empty nanocarriers, and always ≤20 nm (Table 1). This small size should favor their entry in pRBCs, since *Plasmodium* induces new permeation pathways that confer to the host cell an increased permeability to a wide range of particles up to diameters of 50–70 nm.[21] Whereas the unimolecular micelles formed by DHP-bMPA in water (Fig. 8A) had an average diameter around 13.5 nm, DHP-bMPA/drug systems had an average diameter between 12 and 20 nm. Likewise, the loading of antimalarial drugs within HDLDBC-bGMPA nanocarriers resulted in structures with average sizes ranging from 11 to 17 nm (Fig. 8B), whereas the empty nanocarrier had an average size around 13 nm. AFM observation of both CQ-loaded carriers confirmed the formation of these rounded objects (Fig. 8).

***In vitro* antimalarial activity assays.** When the corresponding formulations of HDLDBC-bGMPA and DHP-bMPA
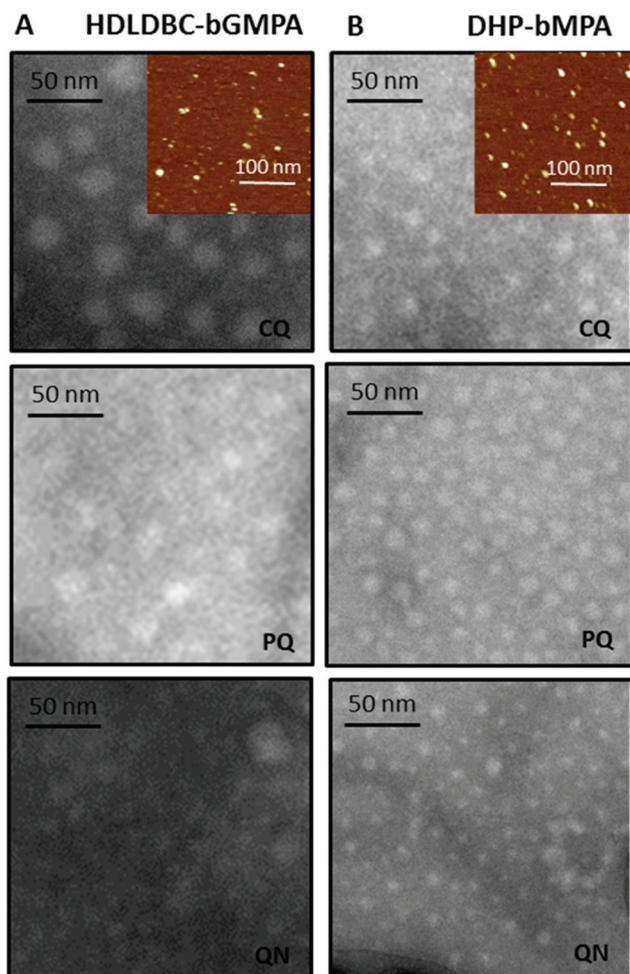
Fig. 8 Negatively stained TEM images of the drug-loaded nanocarriers HDLDBC-bGMPA (A) and DHP-bMPA (B). Insets show AFM images of the corresponding CQ-loaded nanocarriers.

Fig. 9 Growth inhibition assays of *P. falciparum in vitro* cultures treated with CQ, PQ and QN, either free or encapsulated in HDLDBC-bGMPA and DHP-bMPA. In parentheses are indicated the corresponding IC_{50} values.

conjugated with CQ, PQ and QN were tested in growth inhibition assays of *P. falciparum in vitro* cultures, the encapsulated drugs had IC_{50} values comparable to those of the free compounds (Fig. 9), indicating an adequate release of the drugs from the polymers. However, the good targeting of the nanostructures towards pRBCs offered prospects for a better performance of the encapsulated drugs, suggesting that part of the nanoparticle-conjugated compounds might not be adequately released. To explore this possibility, the release dynamics against PBS of CQ encapsulated within HDLDBC-bGMPA and DHP-bMPA was analyzed during three days (Fig. 10). As already described for other dendritic derivatives,[18] CQ was progressively released from both nanocarriers in a process that reached completion in about 24 h; after this time, about 35% of CQ remained stably encapsulated. Modifications of the polymer architecture or chemistry to endow it with more porosity or less affinity for the drugs might contribute to an improved drug release profile.
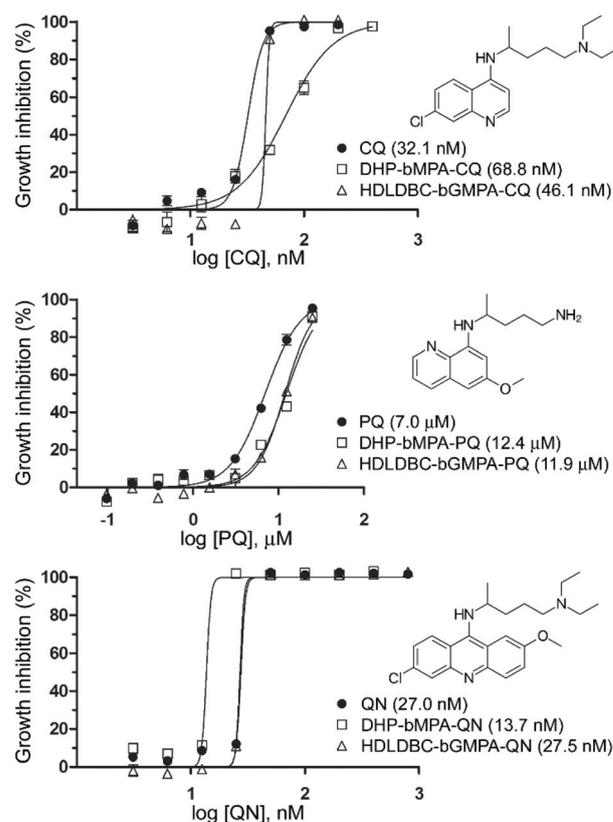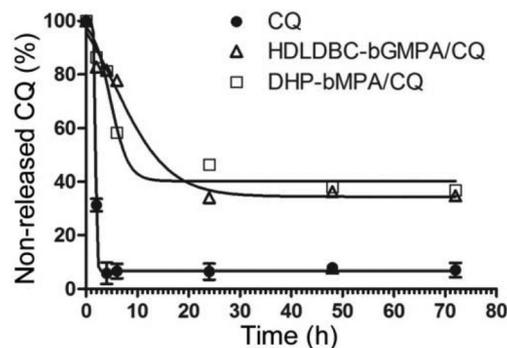

Fig. 10 Release profiles of CQ from the dendrimers DHP-bMPA and HDLDBC-bGMPA at 37 °C.

In vivo antimalarial activity of CQ-loaded nanocarriers

MTD assays indicated that DHP-bMPA and HDLDBC-bGMPA could be safely administered to mice without evident signs of animal distress up to respective doses of at least 37.5 and 120 mg kg^{-1}. For the evaluation of the formulations in an *in vivo* model of malaria, we selected CQ because, being the *in vitro* performance of its encapsulated form *vs.* the free compound similar to that of PQ and QN, this drug had been suc-

cessfully tested in our group as part of different polymeric and liposomal encapsulations.[18,35,38] When polymer-CQ conjugates were administered intravenously (1.9 mg CQ per kg per day for 4 consecutive days) to mice infected with the lethal murine malaria parasite *P. yoelii yoelii* 17XL (PyL) MRA-267, DHP-bMPA-CQ did not improve survival significantly, but animals treated with HDLDBC-bGMPA-CQ survived much longer (3 out of 5 mice lived ≥20 days) than untreated controls, which typically died at day 6 (Fig. 11A and C). One mouse treated with HDLDBC-bGMPA-CQ was actually cured and, when re-infected at day 69 and left untreated, it recovered completely without showing any symptoms of malaria or developing parasitemia above the detection level of microscopy examination. The detection in the plasma of this cured animal of antibodies against *P. yoelii* antigens (Fig. 11B) was consistent with the development of immunity against the disease. Free CQ-treated controls which were administered the same drug concentration were cured in 4 out of 5 animals, which became also resistant to re-infection. Although HDLDBC-bGMPA-encapsulated CQ did not improve the efficacy of such a good drug as CQ, the strategy presented here can be adapted to the targeted drug delivery of other antimalarials, already existing or yet to be discovered.

In vivo, HDLDBC-bGMPA-CQ worked better than DHP-bMPA-CQ, possibly because the former targets all RBCs. The

loading of antimalarial drugs into non-parasitized red blood cells has been described as an efficient approach to significantly reduce parasite survival,[35,36] as long as neither nanocarriers nor drugs affect the natural role of erythrocytes as O_2 and CO_2 transporters. Both dendrimeric structures studied in this work lack significant *in vitro* cytotoxicity and hemolytic activity, suggesting that they will not interfere with the red blood cell physiology. HDLDBC-bGMPA then holds promise for the development of innovative antimalarial prophylactic strategies at the cell level whereby *Plasmodium* would be exposed to drugs since the very first moment after invading a host cell.

The modest *in vivo* efficacy of the encapsulated formulations relative to the free drug is, in part, likely resulting from renal and splenic clearance of the nanoparticles, in addition to their endothelial cell uptake. Nanoparticles must be larger than 20 nm in diameter to avoid filtration by the kidney,[39] and smaller than 100 nm to avoid a specific sequestration by sinusoids in spleen and fenestra of liver, which are approximately 150–200 nm in diameter.[40] Therefore, systemically administered nanoparticles should have diameters from 20 to 100 nm,[41] and overall, literature suggests that nanoparticles in the 50–100 nm size range display the lowest blood clearance rates.[42] Since the average diameter of the dendrimeric nanoparticles used here is just below 20 nm, increasing their size to *ca.* 50 nm might provide an improved pharmacokinetics and better *in vivo* performance.

In addition, upon intravenous administration of nanoparticles, these are coated by a variety of serum proteins which are recognized by the scavenger receptor on macrophage cell surfaces and internalized, leading to a significant loss of nanoparticles from the circulation.[43] The serum proteins binding on the nanoparticles are also termed "opsonins", and the macrophages contributing the major loss of injected dose are also known as the reticuloendothelial system or mononuclear phagocyte system. Reducing protein binding is the key point for developing a long-circulation nanoparticle formulation. To minimize opsonization, the most commonly used strategy is to conjugate onto the surface of the nanoparticles the polyethylene glycol polymer[44] or polyoxazolines,[45] both hydrophilic polymers that provide good steric hindrance for preventing protein binding.

Finally, in addition to expanding blood residence time and reducing unspecific interactions with non-target cells and tissues, a faster targeting dynamics can be conferred to the nanoparticles by coating them with molecules binding pRBCs with certain degree of specificity, as it has been described for heparin.[46,47] Here we have shown that although DHP-bMPA exhibited a remarkable preferential binding to pRBCs *vs.* RBCs, about 40% of pRBCs interacted with this polymer similarly as a fraction of the non-infected erythrocyte population did (Fig. 6). The functionalization of DHP-bMPA-Rho with up to 15% heparin-FITC (w/w) did not affect the targeting specificity of the polymer towards pRBCs (Fig. S3.1†), and it actually favored specific interactions with pRBCs *vs.* RBCs (data not shown). The known activity of
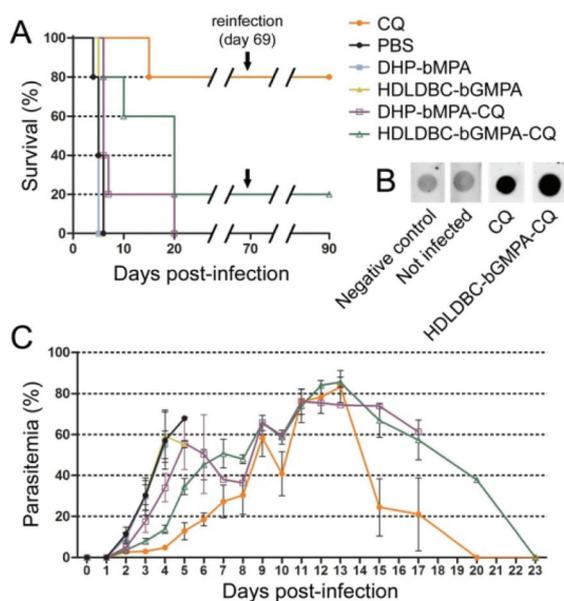

Fig. 11 Four-day blood suppressive antimalarial activity assay of free CQ and of carrier-CQ conjugates. (A) Kaplan–Meier plot of the survival of *P. yoelii yoelii* 17XL (PyL) MRA-267-infected mice treated with 1.9 mg CQ per kg per day for 4 consecutive days, administered intravenously as diphosphate–drug or dendrimer–drug. When all surviving animals had completely cleared *Plasmodium* infection they were re-infected (on day 69) with *P. yoelii* and left untreated. (B) Dot blot for the detection at day 90 in the plasma of surviving animals of antibodies against *P. yoelii*. The negative control was processed substituting PBS for plasma. (C) Parasitemia counts of the different mouse groups until animal death or parasite clearance.

heparin as targeting element of liposomes[47] suggests that its presence on the nanocarrier increased the number of polymers bound to each pRBC. Last but not least, since heparin has antimalarial activity, this result indicates that it can be a constituent of pRBC-targeted multicomponent nanoparticles carrying different types of antimalarial agents.

Conclusions

To eradicate malaria, there is an urgent need for the combination of different strategies working together, because it is unlikely for a single approach to be capable of success. It is important to emphasize the importance of implementing in advance efficient methods of antimalarial drug encapsulation and targeted delivery in order to make a good use of future therapeutic compounds. This should result in a more rational administration regime that could contribute to expand the time during which drugs can be used before resistance evolves. In addition, such strategy might widen the number of chemicals that reach the clinic if eventual unspecific toxicities can be reduced through a targeted delivery approach. The resulting lower overall doses should not trigger pernicious side-effects in the patient while keeping high local doses on the parasite in order to quickly eliminate all the cells of the pathogen, thus reducing the evolution of resistances. Here, we have described micellar carriers based on dendritic macromolecules containing bis-MPA and glycine that hold promise for the development of future antimalarial nanomedicines targeted to both *Plasmodium*-infected and non-infected erythrocytes.

Authors contributions

The manuscript was written through the contributions of all authors. All authors have given approval to the final version of the manuscript.

Conflicts of interest

There are no conflicts to declare.

Acknowledgements

Notes and references

1 World Health Organization, World Malaria Report 2018. http://www.who.int/malaria/publications/world-malaria-report-2018/report/en/, 2018.

2 V. S. Moorthy, R. D. Newman, P. Duclos, J. M. Okwo-Bele and P. G. Smith, *Lancet Infect. Dis.*, 2013, **13**, 280–282.

3 A. Mbengue, S. Bhattacharjee, T. Pandharkar, H. Liu, G. Estiu, R. V. Stahelin, S. S. Rizk, D. L. Njimoh, Y. Ryan, K. Chotivanich, C. Nguon, M. Ghorbal, J. J. Lopez-Rubio, M. Pfrender, S. Emrich, N. Mohandas, A. M. Dondorp, O. Wiest and K. Haldar, *Nature*, 2015, **520**, 683–687.

4 P. L. Alonso and M. Tanner, *Nat. Med.*, 2013, **19**, 150–155.

5 M. Prudêncio, A. Rodriguez and M. M. Mota, *Nat. Rev. Microbiol.*, 2006, **4**, 849–856.

6 A. F. Cowman and B. S. Crabb, *Cell*, 2006, **124**, 755–766.

7 K. S. Griffith, L. S. Lewis, S. Mali and M. E. Parise, *J. Am. Med. Assoc.*, 2007, **297**, 2264–2277.

8 R. G. Feachem, A. A. Phillips, G. A. Targett and R. W. Snow, *Lancet*, 2010, **376**, 1517–1521.

9 P. L. Alonso, *Int. Microbiol.*, 2006, **9**, 83–93.

10 J. P. Daily and J. Clin, *Pharmacol.*, 2006, **46**, 1487–1497.

11 European Science Fundation: ESF Forward Look on Nanomedicine 2005. http://www.nanopharmaceuticals.org/files/nanomedicine.pdf, 2005.

12 M. Saltzman and T. Desai, *Ann. Biomed. Eng.*, 2006, **34**, 270–275.

13 P. Urbán, J. J. Valle-Delgado, E. Moles, J. Marqués, C. Díez and X. Fernàndez-Busquets, *Curr. Drug Targets*, 2012, **13**, 1158–1172.

14 N. Kuntworbe, N. Martini, J. Shaw and R. Al-Kassas, *Drug Dev. Res.*, 2012, **73**, 167–184.

15 P. Urbán and X. Fernàndez-Busquets, *Curr. Med. Chem.*, 2014, **21**, 605–629.

16 M. Selin, L. Peltonen and L. M. J. Bimbo, *J. Drug Delivery Sci. Technol.*, 2016, **34**, 10–20; H. Yang, *Nanomedicine*, 2016, **12**, 309; A. M. Caminade and C. O. Turrin, *J. Mater. Chem. B*, 2014, **2**, 4055–4066; P. Kesharwani, K. Jain and N. K. Jain, *Prog. Polym. Sci.*, 2014, **39**, 268–307.

17 S. García-Gallego, A. M. Nyström and M. Malkoch, *Prog. Polym. Sci.*, 2015, **48**, 85–110.

18 J. Movellan, P. Urbán, E. Moles, J. M. De la Fuente, T. Sierra, J. L. Serrano and X. Fernàndez-Busquets, *Biomaterials*, 2014, **35**, 7940–7950.

19 R. D. Sikwal, R. S. Kalhapure and T. Govender, *Eur. J. Pharm. Sci.*, 2017, **97**, 113–134.

20 B. S. Bolu, R. Sanyal and A. Sanyal, *Molecules*, 2018, **23**, 1570–1595.

21 I. D. Goodyer, B. Pouvelle, T. G. Schneider, D. P. Trelka and T. F. Taraschi, *Mol. Biochem. Parasitol.*, 1997, **87**, 13.

22 A. Fonseca, M. A. Gil and P. M. Simões, *Prog. Polym. Sci.*, 2014, **39**, 1291–1311.

23 M. Winnacker and B. Rieger, *Polym. Chem.*, 2016, **7**, 7039–7046.

24 A. Lancelot, R. González-Pastor, R. Clavería-Gimeno, P. Romero, O. Abián, P. Martín-Duque, J. L. Serrano and T. Sierra, *J. Mater. Chem. B*, 2018, **6**, 3956–3968.

25 A. Lancelot, R. González-Pastor, A. Concellón, T. Sierra, P. Martín-Duque and J. L. Serrano, *Bioconjugate Chem.*, 2017, **28**, 1135–1150.

26 M. C. A. Stuart, J. C. van de Pas and J. B. F. N. Engberts, *J. Phys. Org. Chem.*, 2005, **18**, 929–934.

27 I. Jiménez-Pardo, R. González-Pastor, A. Lancelot, R. Clavería-Gimeno, A. Velázquez-Campoy, O. Abián, M. B. Ros and T. Sierra, *Macromol. Biosci.*, 2015, **15**, 1381–1391.

28 P. Urbán, J. Estelrich, A. Cortés and X. Fernàndez-Busquets, *J. Controlled Release*, 2011, **151**, 202–211.

29 S. L. Cranmer, C. Magowan, J. Liang, R. L. Coppel and B. M. Cooke, *Trans. R. Soc. Trop. Med. Hyg.*, 1997, **91**, 363–365.

30 C. Lambros and J. P. Vanderberg, *J. Parasitol.*, 1979, **65**, 418–420.

31 D. A. Fidock, P. J. Rosenthal, S. L. Croft, R. Brun and S. Nwaka, *Nat. Rev. Drug Discovery*, 2004, **3**, 509–520.

32 J. Marques, E. Vilanova, P. A. S. Mourão and X. Fernàndez-Busquets, *Sci. Rep.*, 2016, **6**, 24368.

33 G. R. Newkome, C. N. Moorefield, G. R. Baker, M. J. Saunders and S. H. Grossman, *Angew. Chem., Int. Ed. Engl.*, 1991, **30**, 1178–1180.

34 X. Fan, Z. Lia and X. J. Loh, *Polym. Chem.*, 2016, **7**, 5898–5919.

35 E. Moles, P. Urbán, M. B. Jiménez-Díaz, S. Viera-Morilla, I. Angulo-Barturen, M. A. Busquets and X. Fernàndez-Busquets, *J. Controlled Release*, 2015, **210**, 217–229.

36 E. Moles and X. Fernàndez-Busquets, *Future Med. Chem.*, 2015, **7**, 837–840.

37 E. Moles, S. Galiano, A. Gomes, M. Quiliano, C. Teixeira, I. Aldana, P. Gomes and X. Fernàndez-Busquets, *Biomaterials*, 2017, **145**, 178–191.

38 P. Urbán, J. J. Valle-Delgado, N. Mauro, J. Marques, A. Manfredi, M. Rottmann, E. Ranucci, P. Ferruti and X. Fernàndez-Busquets, *J. Controlled Release*, 2014, **177**, 84–95.

39 D. Venturoli and B. Rippe, *Am. J. Physiol.: Renal Physiol.*, 2005, **288**, F605–F613.

40 X. Duan and Y. Li, *Small*, 2012, **9**, 1521–1532.

41 M. E. Davis, Z. Chen and D. M. Shin, *Nat. Rev. Drug Discovery*, 2008, **7**, 771–782.

42 F. Alexis, E. Pridgen, L. K. Molnar and O. C. Farokhzad, *Mol. Pharm.*, 2008, **5**, 505–515.

43 M. C. Woodle, M. S. Newman and J. A. Cohen, *J. Drug Targeting*, 1994, **2**, 397–403.

44 S. D. Li and L. Huang, *Mol. Pharm.*, 2008, **5**, 496–504.

45 R. B. Restani, J. Conde, R. F. Pires, P. Martins, A. R. Fernandes, P. V. Baptista, V. D. B. Bonifácio and A. Aguiar-Ricardo, *Macromol. Biosci.*, 2015, **15**, 1045–1051.

46 X. Fernàndez-Busquets, *Future Med. Chem.*, 2013, **5**, 737–739.

47 J. Marques, E. Moles, P. Urbán, P. Prohens, M. A. Busquets, C. Sevrin, C. Grandfils and X. Fernàndez-Busquets, *Nanomedicine*, 2014, **10**, 1719–1728.